

Spectroscopic data, spin-orbit functions, and revised analysis of strong perturbative interactions for the $A^1\Sigma^+$ and $b^3\Pi$ states of RbCs

O. Docenko,¹ M. Tamanis,¹ R. Ferber,¹ T. Bergeman,² S. Kotochigova,³ A. V. Stolyarov,⁴ Andreia de Faria Nogueira,⁵ and C. E. Fellows⁵

¹Laser Center, University of Latvia, 19 Rainis Boulevard, Riga LV-1586, Latvia

²Department of Physics and Astronomy, SUNY, Stony Brook, New York 11794-3800, USA

³Department of Physics, Temple University, Philadelphia, Pennsylvania 11922, USA

⁴Department of Chemistry, Moscow State University, GSP-2 Leninskie gory 1/3, Moscow 11992, Russia

⁵Laboratório de Espectroscopia e Laser, Universidade Federal Fluminense, Campus da Boa Viagem, Niterói, RJ 24210-340, Brazil

(Received 12 December 2009; published 16 April 2010)

The current interest in producing ultracold RbCs molecules by optical excitation from weakly bound Feshbach resonances and stimulated decay to the absolute ground state requires detailed analyses of the intermediate excited states. In this study, we present two sets of experimental Fourier-transform spectroscopic data of the $A^1\Sigma^+ - b^3\Pi$ complex. The $A-b$ mixed vibrational levels are the most likely candidates to be intermediates in the molecular formation. The more recent and more accurate data set is from mixed $A-b \rightarrow X$ transitions, while the second is derived in large part from $(4)^1\Sigma^+ \rightarrow A-b$ emission and extends to higher $A-b$ energy levels. From a detailed analysis of the spectroscopic data we obtain term values which allow one to construct potentials and spin-orbit functions. Vibrational numbering of the A state has been raised by one quantum over a previous report [T. Bergeman *et al.*, Phys. Rev. A **67**, 050501 (2003)] while the numbering of the b state is established with a considerable degree of certainty with help of data on the $^{85}\text{Rb}^{133}\text{Cs}$ and $^{87}\text{Rb}^{133}\text{Cs}$ isotopomers. In addition, we have performed calculations of spin-orbit functions by two distinct methods. The fitted spin-orbit coupling matrix element between the two $\Omega^p = 0^+$ states, $A^1\Sigma^+$ and $b^3\Pi_{0,+}$, happens to agree rather well with the results from both of these methods, while for the diagonal $b^3\Pi$ state spin-orbit function, the fitted function agrees fairly well with that obtained by the other method.

DOI: 10.1103/PhysRevA.81.042511

PACS number(s): 33.20.Kf, 31.15.aj, 31.50.Df

I. INTRODUCTION

The lowest excited states of the alkali-metal dimers are of interest as gateway states for the excitation of higher states [1] and recently as intermediate states in the production of cold molecules from cold atoms formed by photoassociation or from Feshbach resonances [2–4]. In the heavier alkali-metal dimers, the $A^1\Sigma^+_{(u)}$ and $b^3\Pi_{(u)0}$ states (where the u subscript applies only to homonuclear species) are also of interest in regard to the challenges of modeling strong spin-orbit coupling interactions.

Cold heteronuclear alkali-metal diatomic molecules have been of especial interest [5] because their ground-state dipole moment leads to dipole-dipole interactions, for example, in a molecular Bose-Einstein condensate. Also because of this property, cold RbCs molecules in particular have been proposed as possible quantum qubits for use in a quantum computer [6]. After intense effort, cold ground state RbCs [7], KRb [8], and LiCs [9] molecules have been produced, and there continues to be interest in efficient ways of producing translationally cold molecules in the lowest rovibrational level of the ground electronic state. The scheme first used for RbCs [7,10,11] happened to bypass the $A^1\Sigma^+$ and $b^3\Pi$ states. However, recently after Feshbach resonances were observed in this species [12], there have been efforts [13] to excite from one of the Feshbach resonance states up to mixed $A-b$ levels and then down to low levels of the $X^1\Sigma^+$ state by STIRAP steps, as performed with Cs_2 [4], KRb [8], and Cs_2 molecules in a lattice [14]. Such methods, as well as other proposed chirped laser methods [15], make it imperative to improve the knowledge of the structure of the lowest excited states of RbCs, namely the A and b states.

In general, questions about the energy levels and spin-orbit interactions among the lowest excited states of the heteronuclear alkali-metal dimers have attracted considerable attention, and there has been impressive progress in data acquisition and analysis. Studies of broadest scope have considered all states dissociating to the lowest $^2S + ^2P$ limit, namely $A^1\Sigma^+$, $b^3\Pi$, $c^3\Sigma^+$, and $B^1\Pi$. However, this broader goal has been pursued only in a preliminary manner for NaK [16] and even more tentatively for RbCs [17]. Studies focusing on the A and b states of heteronuclear alkali-metal dimers include work on NaK by Refs. [18–21] and work on NaRb [22,23], NaCs [24], and RbCs [25]. For NaRb and NaCs, vibrational assignments of both states have been reliably determined, and the perturbative interactions have been modeled to an accuracy of 0.01 cm^{-1} or better. Higher-order spin-orbit effects were included in Ref. [24], and there was quite good agreement between empirically extracted and *ab initio* potential and spin-orbit functions.

Studies of the A and b states of the homonuclear dialkali-metal species Li_2 [26–29], Na_2 [30–34], K_2 [35–39], and Rb_2 [40,41] have also contributed to the development of experimental and theoretical methods applicable to heteronuclear alkali-metal dimers. For Na_2 [34], data now extend almost continuously from the lowest vibrational levels to the atomic limit.

In this report, we present experimental observations on RbCs that give a change of vibrational numbering of the $A^1\Sigma^+$ state as well as of the $b^3\Pi$ state, relative to the previously published values [25]. We have combined data from the University of Latvia, Riga, with older data, assigned in Rio de Janeiro, Brazil, which were obtained more than 10 years

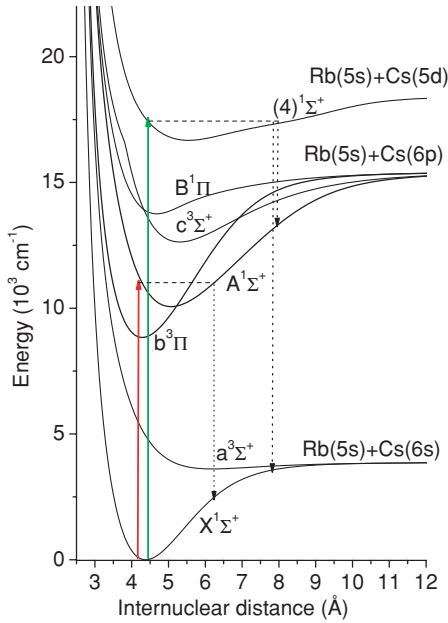


FIG. 1. (Color online) Selected lowest electronic states of RbCs [42] along with the laser excitation/FTS fluorescence observation used in this study. There are measurements of fluorescence from mixed A - b levels to the X state in both data sets. In addition, fluorescence from the $(4)^1\Sigma^+$ state to X state levels and to mixed A - b levels is contained in the data from Brazil.

ago in the Laboratoire Aimé Cotton (LAC), Orsay, France. The primary goal of the latter one had been to characterize the X state rather than the excited states. The older data had been transported to Brazil only in the form of printed scans which resulted in a deterioration of the line measurement accuracy. In combining the two data sets, we have given standard errors in the ratio 4:1 (old:new), which reflects the scale of the residuals. However, the older data set is useful because it extends to higher energies. The combined data yield a determination of the spin-orbit function that couples $A^1\Sigma^+$ and $b^3\Pi_{0+}$ and also the spin-orbit splitting between $b^3\Pi_1$ and $b^3\Pi_{0+}$. Figure 1 summarizes the transitions used in this study, with potentials from Ref. [42].

The theoretical model used here shares much the same Hamiltonian elements as in previous studies cited above. In summary, Sec. II presents the experimental techniques, Sec. III the data analysis, Sec. IV discusses the *ab initio* calculations of the spin-orbit functions, and Sec. V concludes with a presentation of the fitted parameters and a discussion of the implications of this work.

II. EXPERIMENTAL DATA

A. Data from Brazil/LAC

Experimental data were obtained by Fourier-transform spectroscopy (FTS) and laser-induced fluorescence (LIF). The production of RbCs molecules and the experimental setup will not be described here and can be found elsewhere [43]. The fluorescence was induced by two different monomode lasers; a Ti:sapphire oscillating in the $11\,000\text{ cm}^{-1}$ region and a dye laser (operating with DCM and Rh6G dyes) oscillating in the $17\,000\text{ cm}^{-1}$ region. The fluorescence was

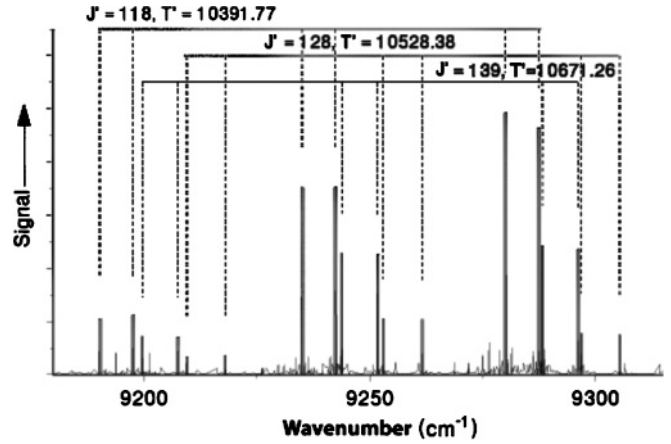


FIG. 2. A portion of the fluorescence line spectrum from mixed $A^1\Sigma^+-b^3\Pi_0$ levels to $X^1\Sigma^+$ state levels on excitation with laser wavelength of 1006.461 nm . Each doublet consists of $P(J'+1)$ and $R(J'-1)$ lines. In this plot, $v'' = 20-18$ for $J' = 118$; $= 24-22$ for $J' = 128$; and $= 24-22$ for $J' = 139$. T' denotes the excited-state term value and is given in cm^{-1} .

focused into the entrance iris of a 2-m optical path length Fourier-transform spectrometer constructed in the Laboratoire Aimé Cotton, Orsay, France, and the spectra were recorded in three optical ranges. For the first data set, fluorescence was induced by the Ti:sapphire lines, and recorded in the $11\,000$ to 8000 cm^{-1} range, to observe the transition from the mixed $A^1\Sigma^+-b^3\Pi$ electronic states (henceforth called A - b) to the $X^1\Sigma^+$ electronic ground state. An example of such spectra is shown in Fig. 2. The second data set was obtained in order to assign rotational quantum numbers for $(4)^1\Sigma^+$ levels. It consisted of fluorescence induced by the monomode dye laser, observed in the region between $17\,130$ and $16\,000\text{ cm}^{-1}$, yielding data on $(4)^1\Sigma^+ \rightarrow X^1\Sigma^+$ transitions (see Fig. 1). The third data set, as shown in Fig. 3, also induced by the monomode dye laser and using exactly the same laser lines used in the previous step, was recorded in the region from 8500 to 5565 cm^{-1} , yielding spectra from the $(4)^1\Sigma^+ \rightarrow A$ - b transition.

With the $(4)^1\Sigma^+ \rightarrow X^1\Sigma^+$ transition lines, the P-R intervals in the fluorescence spectra to the electronic ground state allowed an unambiguous J' numbering so that in the third step, the $(4)^1\Sigma^+ \rightarrow A/b$ transition, the J' values were already assigned. Assignment of transitions in RbCs was facilitated by previous data obtained on Rb_2 and Cs_2 spectra in the same region.

In summary, some 1175 unique term values were obtained from FTS measurements of fluorescence from A - b levels to the X state or by direct measurements of the fluorescence from the $(4)^1\Sigma^+$ state to A - b state levels. Also 374 term values (some duplicating the above) were obtained from emission from levels of the RbCs $(4)^1\Sigma^+$ state that were populated by collisional transfer (rotational relaxation) from levels originally excited by the dye laser. To deduce A - b term values from these data, term values for the $(4)^1\Sigma^+$ state were obtained by least squares fit of all available data on this state, as reported in Ref. [44]. Rotational relaxation extended the range of J values for certain scans in both data sets 1 and 3.

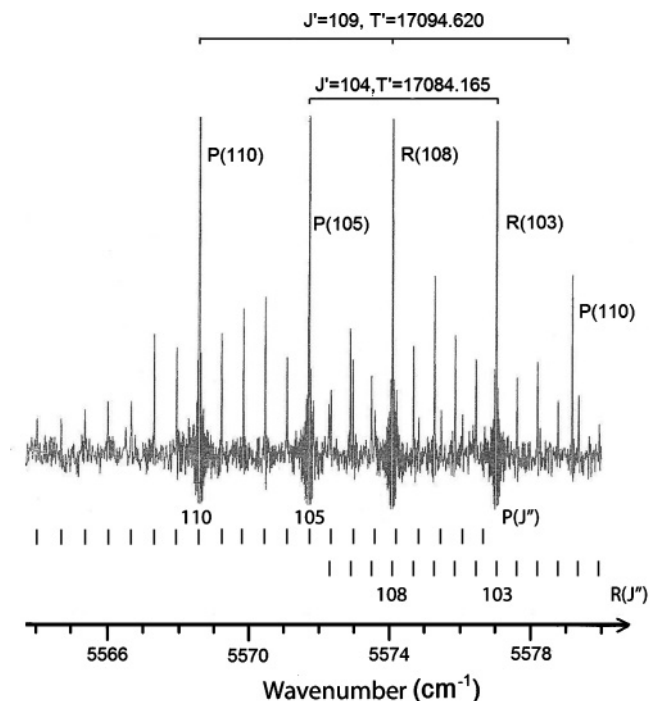


FIG. 3. A portion of the fluorescence spectrum from the $(4) \ ^1\Sigma^+$ state to mixed $A \ ^1\Sigma^+ - b \ ^3\Pi_{0+}$ levels.

B. Data from Riga, University of Latvia

In the experiments performed in Latvia, RbCs molecules were produced in a stainless steel heat pipe similar to the one developed for NaCs [24,45] studies. The heat pipe was filled with 10 g Rb and approximately 6 g Cs. An ampoule with Cs was loaded into the side container [45] at the central part of the heat pipe. Typical operating pressure of Ar buffer gas was 2–3 mbar. During the experiments the heat pipe was kept at temperature of about 285°C by a Carbolite furnace.

The experimental arrangement was similar to the one used for NaCs and KCs studies [24,46]. LIF was spectrally analysed with a Fourier-transform spectrometer, Bruker IFS 125HR. For fluorescence detection we used an $\text{In}_x\text{Ga}_{1-x}\text{As}$ diode operated at room temperature. The resolution of the spectrometer was typically set to 0.03 cm^{-1} . In order to ensure a sufficient signal-to-noise ratio for the lines of medium strength, the number of scans for each recorded spectrum was typically 20 and averaging over a number of repeated measurements was applied in some cases.

For studies of the A - b complex we applied a direct excitation of its levels by diode lasers followed by observation of the A - $b \rightarrow X \ ^1\Sigma^+$ LIF, see Fig. 1. Two laser diodes, namely 1020 nm (LD-1020-0400-1 from Toptica Photonics) and 1060 nm (L1060P100J from Thorlabs), were used. The power of the lasers at the entrance of the heat pipe were typically about 30 mW for the 1060-nm diode and 50 mW for the 1020-nm diode. The lasers were tuned in the ranges $[9700, 9860]$ and $[9360, 9510] \text{ cm}^{-1}$, respectively. Measurements were made at fixed laser frequencies which excited strong fluorescence signal controlled at reduced resolution in the preview mode regime of the spectrometer. Excitation frequencies were measured by a wavemeter (HighFinesse WS6) with about 0.015 cm^{-1} accuracy.

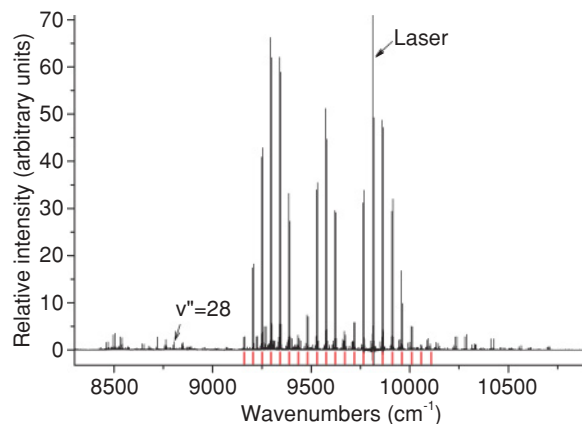


FIG. 4. (Color online) Example of LIF spectrum excited by laser line 9811.933 cm^{-1} . Red vertical lines indicate $^{85}\text{Rb}^{133}\text{Cs}$ LIF progression excited in the transition $(v'_A = 2, J' = 83)A \ ^1\Sigma^+ \leftarrow (v'' = 6, J'' = 84)X \ ^1\Sigma^+$. Intensity distribution of LIF progression clearly indicates the $v'' = 2$ numbering in the A state. Other weaker lines seen in the spectrum belong to transitions in RbCs too. Transitions in Rb_2 and Cs_2 are not seen in the scale of the figure.

Lasers applied in the present experiments excited efficiently not only the RbCs molecules but the Cs_2 and Rb_2 molecules as well, thus creating in the observed spectra a dense structure, governed by rather small line spacings in these heavy alkali-metal dimers. Nevertheless, high-resolution spectra allowed us to perform assignment unambiguously. An example of spectrum is shown in Fig. 4.

The identification and assignment of fluorescence bands to the $X \ ^1\Sigma^+$ state of RbCs was straightforward, using Dunham coefficients from Ref. [43]. For the A - X transitions we observed only doublet progressions according to the selection rules. In a number of cases wide groups of satellite lines appeared around the strong LIF lines due to collision induced distribution of the population of the directly excited rovibronic level over neighboring rotational levels. Moreover, levels of the interaction partner are sometimes populated as well, therefore allowing us to obtain the manifold of both mixed singlet and triplet levels at one shot, see e.g. Fig. 5. Such groups of lines usually do not have a clear central line and are located in a different part of the spectrum comparing to LIF line satellites. Using rotational satellites, it was also possible to predict new excitations of different J' levels thus allowing the rotational ladder to be discovered step by step. Assigning of rotational satellites was complicated by the presence of local perturbations, see e.g. Fig. 6, which, however, gave very valuable direct information on the splitting of levels in the A - b complex.

The energies of the A - b complex levels were obtained by adding transition wavenumbers to the energy of the respective X state level calculated with the Dunham coefficients from Ref. [43]. The reported value for a given A - b rovibrational level was obtained by averaging over term values from transitions to different ground-state levels. The uncertainty of the derived energy values is, however, mostly limited by the Doppler shift: if fluorescence is induced by a single-mode laser which is not tuned exactly to the center of the absorption profile and observation is parallel to the laser beam then all transition frequencies will be Doppler shifted. The Doppler

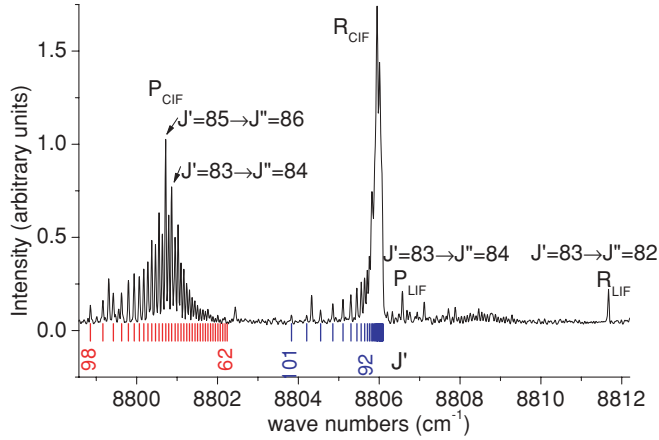


FIG. 5. (Color online) Example of fluorescence from collisionally populated rotational levels of the mixing partner which was not directly excited by the laser (P_{CIF} and R_{CIF} lines, where CIF states for collisionally induced fluorescence). The corresponding level populated by direct excitation is ($v'_A = 2$, $J' = 83$) in $^{85}\text{Rb}^{133}\text{Cs}$ the LIF spectrum of which is shown in Fig. 4. Transitions to $v'' = 28$ are shown. One can see also corresponding weak transitions from the directly populated level (P_{LIF} and R_{LIF} lines). Numbers at vertical bars denote the rotational quantum number of the upper state.

broadening at our working temperatures and spectral range is ca. 0.012 cm^{-1} and we estimate our maximal A - b energy level uncertainty as 0.01 cm^{-1} .

Note that Ref. [43] does not contain the Y_{00} member of the Dunham expansion. Since we want to relate all our potential energy curves to the bottom of the ground-state potential we need to add the Y_{00} value to the energies obtained from the Dunham expansion of Table 1 of Ref. [43]. Calculated Y_{00}

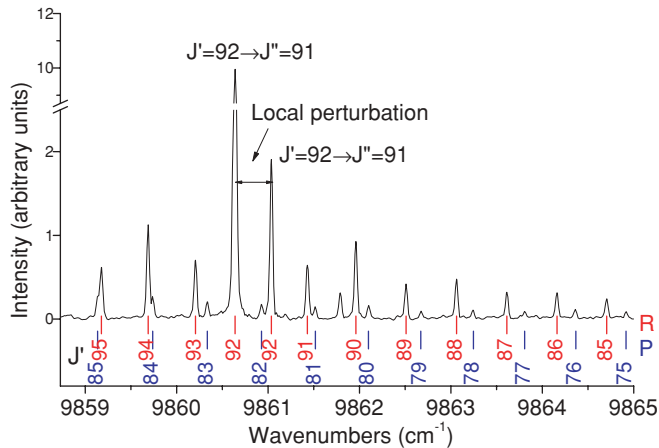


FIG. 6. (Color online) Example of local perturbation in the A - $b \rightarrow X$ spectrum. LIF was excited in the $^{85}\text{Rb}^{133}\text{Cs}$ molecule by laser line 9806.284 cm^{-1} in transition A - b ($v_A = 2$, $J' = 92$) \leftarrow X ($v'' = 6$, $J'' = 93$). The most intense line corresponds to the LIF line A - b ($v_A = 2$, $J' = 92$) \rightarrow X ($v'' = 5$, $J'' = 91$). On the right-hand side one can see the line which also originates from $J' = 92$, but from other mixed level of the A - b complex. Numbers at vertical bars denote the rotational quantum number of the upper state. The upper bars denote R lines and lower bars P lines. Term values derived from these perturbed spectral lines are plotted in Fig. 14 below.

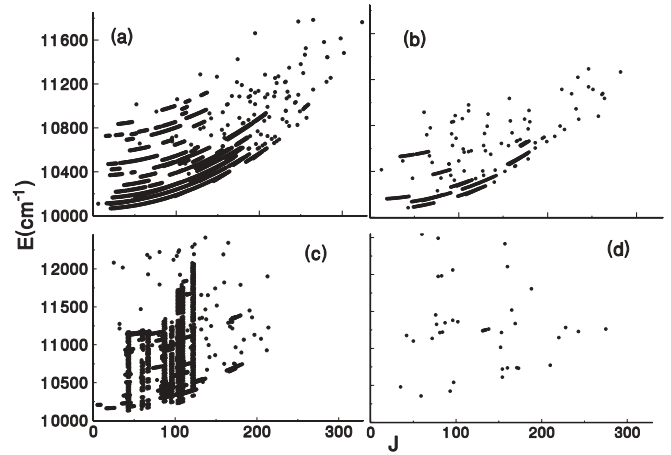


FIG. 7. A summary of the data obtained in this study and used in the analysis. (a) and (b) are from Riga; (c) and (d) are from Brazil. (a) and (c) are data from $^{85}\text{Rb}^{133}\text{Cs}$, while (b) and (d) are data from $^{87}\text{Rb}^{133}\text{Cs}$.

values are -0.0089 cm^{-1} for $^{85}\text{Rb}^{133}\text{Cs}$ and -0.0088 cm^{-1} for $^{87}\text{Rb}^{133}\text{Cs}$.

Vibrational numbering of the $A^1\Sigma^+$ state was revised from previous work [25] based on observations in Riga of the intensity distribution in fluorescence progressions. We have in fact observed transitions from $v' = 0$ level which is one vibrational quantum lower than the previously assigned $v' = 0$ of the A state. Thus the previous vibrational numbering has been increased by one.

Overall from Riga measurements 1756 term values of the A - b complex of $^{85}\text{Rb}^{133}\text{Cs}$ and 439 term values of $^{87}\text{Rb}^{133}\text{Cs}$ have been obtained in the range of $v_A = 0$ –20 and $J' = 6$ –324 and energy range $10\,066$ – $11\,784\text{ cm}^{-1}$. (At the high energy limit, the intense mixing between $A^1\Sigma^+$ and $b^3\Pi_{0+}$ makes the assignment of vibrational quantum numbers problematical, as discussed below.) A list of excited $X \rightarrow A$ transitions, measured LIF and rotational relaxation lines and derived A - b term values are given in EPAPS tables [47].

C. Summary of data

Figure 7 shows the range of term values of both isotopomers and from both sources used in this study. The energy zero in this and all other plots and data tables in this report is the minimum of the ground-state potential. The experimental term values span the range $10\,066$ to $12\,500\text{ cm}^{-1}$ above the X state minimum.

III. ANALYSIS OF THE DATA

A. Hamiltonian elements

The molecular Hamiltonian [48]

$$H = H_{BO} + H_K + H_{so} + H_{rot}, \quad (1)$$

includes the Born-Oppenheimer potentials H_{BO} , radial kinetic energy H_K , nuclear rotation H_{rot} , and spin-orbit interaction H_{so} . Hyperfine interactions can be ignored in the Hamiltonian as hyperfine structure has not yet been observed.

Most of the observed term values could be identified as mixtures of $A^1\Sigma^+$ levels and $b^3\Pi_{0+}$ levels. Because all observed transitions were from $^1\Sigma^+$ states, only levels of

parity $(-1)^J$ (e symmetry) were observed. Only a few levels were found to have significant ${}^3\Pi_1$ character and no levels with significant ${}^3\Pi_2$ character were identified. Customarily, the potential energy of a ${}^3\Pi_0$ state would be represented by $V({}^3\Pi_1) - \Delta_d$, where Δ_d is the diagonal ${}^3\Pi$ spin-orbit interaction. However, in view of the very limited information on the ${}^3\Pi_1$ potential itself, our ${}^3\Pi_0$ potential contains the spin-orbit function implicitly. When ${}^3\Pi_1$ and ${}^3\Pi_2$ levels are considered, the matrix elements of $H_V + H_{so} + H_{rot}$ were taken to be [48]:

$$\begin{aligned}
\langle {}^1\Sigma^+ | H | {}^1\Sigma^+ \rangle &= V({}^1\Sigma^+) + (x+2)B, \\
\langle {}^3\Pi_{0+} | H | {}^3\Pi_{0+} \rangle &= V({}^3\Pi_{0+}) + (x+2)B, \\
\langle {}^3\Pi_1 | H | {}^3\Pi_1 \rangle &= V({}^3\Pi_{0+}) + \Delta_{1d} + (x+2)B, \\
\langle {}^3\Pi_2 | H | {}^3\Pi_2 \rangle &= V({}^3\Pi_{0+}) + \Delta_{1d} + \Delta_{2d} + (x-2)B, \\
\langle {}^1\Sigma^+ | H | {}^3\Pi_{0+} \rangle &= -\Delta_{od}, \\
\langle {}^3\Pi_0 | H | {}^3\Pi_1 \rangle &= -\sqrt{2x}B, \\
\langle {}^1\Sigma^+ | H | {}^3\Pi_{1+} \rangle &= -\sqrt{2x}B\xi, \\
\langle {}^3\Pi_1 | H | {}^3\Pi_2 \rangle &= -\sqrt{2(x-2)}B,
\end{aligned} \tag{2}$$

where $x = J(J+1)$ and $H^T = H$, where H^T is the transpose of H . In the above, $V({}^1\Sigma^+)$, $V({}^3\Pi)$, Δ_{od} (off-diagonal), Δ_{1d} , Δ_{2d} , and $B = \hbar^2/2\mu R^2$ are functions of internuclear distance R (μ is the reduced mass). Δ_{1d} is the $\Omega = 1-0^+$ interval of the b state, and Δ_{2d} is the $\Omega = 2-1$ interval. The parameter ξ arises from a second-order spin-orbit effects, as discussed in Ref. [24].

Initially, the least-squares fitting was performed with a 2×2 Hamiltonian matrix, including simply the $\Omega = 0^+$ manifolds and the off-diagonal spin-orbit coupling term, Δ_{od} . Next a 3×3 Hamiltonian included ${}^3\Pi_1$ levels and Δ_{1d} . Finally fits were made with a four-channel Hamiltonian. Although ${}^3\Pi_2$ components were not directly observed, they affected the fitted parameters through the terms coupling with ${}^3\Pi_1$ and thus indirectly to ${}^3\Pi_{0+}$.

Because the spin-orbit coupling function between the $A {}^1\Sigma^+$ and $b {}^3\Pi_0$ states of RbCs is larger than the vibrational intervals, traditional band-by-band analysis of the perturbative effects is impractical. Our analysis utilizes the discrete variable representation (DVR) [49] to form a Hamiltonian matrix over mesh points in R , the internuclear distance, and over the relevant channels. Eigenvalues of this matrix are the term values, many of which can be matched with experimental data. The kinetic energy operator is a dense matrix over the mesh points in R for each channel and represents d^2/dR^2 as accurately as possible for the given discrete mesh. The scaling function of Ref. [50] is used to minimize the number of mesh points. The potential energies in each channel are represented by diagonal terms in the Hamiltonian matrix, while spin-orbit or Coriolis coupling terms are off-diagonal in channel number but diagonal in the mesh index. For additional details on the numerical methods, please see Ref. [41]. The potential parameters are adjusted by least-squares fitting procedures to minimize the variance, the sum of the residuals each weighted by the inverse square of the experimental uncertainty.

In this report, as in other recent studies, we have adopted the ‘‘Hannover’’ form [51] for the bound part of each

TABLE I. Left and right potential transition points, in \AA , and the potential energies at these points, in cm^{-1} .

	$A {}^1\Sigma^+$	$b {}^3\Pi_{0+}$
R_L	3.934	3.247
$V(R_L)$	12460.6	12332.5
R_R	7.465	6.404
$V(R_R)$	12540.3	12422.0

potential:

$$V_B(R) = T_e + \sum_{i=2}^l a_i \left(\frac{R - R_e}{R + bR_e} \right)^i, \tag{3}$$

In this work, we have relied on Eq. (3) over the range of turning points and energies covering the data. For R less than R_L , the form $\alpha/R^6 + \beta$ was used for each potential, where R_L is chosen such that $V(R_L)$ lies above the highest data points. Similarly for the large R regime, the transition points, R_R , are chosen such that $V(R_R)$ exceeded the observed term values in energy. The potential form used at large R was based on the hope of eventually including data near the dissociation limit, for which the long-range expansion, $V_{disp} = -\sum_{n=6,8,\dots} C_n/R^n$ would be appropriate. This potential form would apply beyond $R = 13 \text{\AA} = R_{LR}$ [52], where overlap of the atomic wave functions is no longer significant. However, since the outer turning points for the highest observed term values were for $R \approx 7.3 \text{\AA} < R_{LR}$, the form V_{disp} could not be applied directly. Instead, an interpolation was performed between the potentials as given in Eq. (3) and potentials of the form V_{disp} given above, with C_n coefficients from Ref. [53]. A four-term expansion in R^{-n} , where $n = 6, 8, 10, 12$ was formed to match the potentials and their derivatives at both $R = R_R$ and at $R = R_{LR}$. Table I gives the $R_{L,R}$ and $V(R_{L,R})$ values. The fitted a_i parameters for both the A and b states are given in Table II. Further details are given in the EPAPS file [47].

TABLE II. Fitted parameters for the RbCs $A {}^1\Sigma^+$ and $b {}^3\Pi_0$ potentials, as used in the form given in Eq. (1). R_e is in \AA , b and ξ are dimensionless, and all other parameters are in cm^{-1} . Numbers in square brackets indicate power of 10.

	$A {}^1\Sigma^+$	$b {}^3\Pi_0$
R_e	5.123914826879	4.338566790508
b	0.01250000000	-0.20250000000
T_e	0.9996467787015[4]	0.8732543511114[4]
a_2	0.2929101955522[5]	0.2378289841686[5]
a_3	-0.2436921592699[4]	0.2859121627122[5]
a_4	-0.2918270666841[5]	-0.2062113364666[5]
a_5	-0.2276287447081[5]	-0.2414988488104[6]
a_6	0.1899296125684[6]	0.8608649875781[5]
a_7	0.1085397339835[7]	0.1473564254061[7]
a_8	-0.4024803153907[7]	-0.6646913623082[5]
a_9	-0.7622096545307[7]	-0.4195125971590[7]
a_{10}	0.2925341147099[8]	-0.2503690400901[7]
a_{11}	-0.1524750618023[8]	0.2664864368812[6]
ξ		-3.40388558

For Δ_{1d} and Δ_{od} , our objective was to obtain purely empirical functions to compare with *ab initio* results. For this purpose a Morse function form was employed, based on the previous studies of alkali-metal dimers exhibiting spin-orbit functions with a dip as a function of R , due to loss of p character in the wave function between $R = \infty$ and the united atom limit, $R = 0$ (see, for example, [23,24,41]):

$$\Delta_i(R) = P_i(1) + (P_i(4) - P_i(1)) \times \{1 - \exp[P_i(2)(P_i(3) - R)]\}^2; \quad i = 1d, 2d, od. \quad (4)$$

$P_i(4)$ is determined by the Cs 6^2P atomic spin-orbit splitting, $\Delta_a = 554.0389 \text{ cm}^{-1}$ [54]: $P_{1d}(4) = P_{2d}(4) = \Delta_a/3$; $P_{od}(4) = \sqrt{2}\Delta_a/3$. The usefulness of expressions of the simple form (4) lies in the circumstance that the experimental data sample only a small range of R values, so that the three adjustable parameters are adequate for most purposes in fitting the data. However, outside the region sampled by the data, the empirical Morse-type functions will deviate from correct spin-orbit interaction functions.

If the second-order spin-orbit shifts for $b^3\Pi_1$ are approximately -4 cm^{-1} , as discussed below, then the ${}^3\Pi_{2-3}\Pi_1$ interval will be about 8 cm^{-1} greater than the ${}^3\Pi_{1-3}\Pi_{0+}$ interval. Hence we took $P_{2d}(1)$ to be 8 cm^{-1} greater than the fitted value of $P_{1d}(1)$ obtained from observations of several $b^3\Pi_1$ levels. Values for other P_{2d} parameters were taken to be the same as the P_{1d} parameters.

B. Fitted potentials and rovibrational structure

The vibrational numberings need to be established before potentials can be constructed. The vibrational numbering of the A state is discussed above. For the $b^3\Pi_{0+}$ state, the sample data obtained in Riga for ${}^{87}\text{Rb}{}^{133}\text{Cs}$ made a decisive determination feasible. Due to the strong mixing with $A^1\Sigma^+$, the isotopomeric shift in itself is not a reliable indicator. However, fits to the data with varying $T_e(b^3\Pi_{0+})$ yielded variances that favored one vibrational numbering over other possibilities by at least a factor of 10. The optimum vibrational numbers for $b^3\Pi_{0+}$ are one less than in Ref. [25]. The determination of vibrational numbering for $b^3\Pi_1$ levels is discussed below.

Fitted potentials are shown in Fig. 8. Our best fit results give an rms residual of 0.019 cm^{-1} for the data from Riga and 0.079 cm^{-1} for the LAC/Brazil data. Residuals from the best fit are shown in Fig. 9.

The energy level structure as observed and calculated from fitted parameters is displayed in several figures that follow, for various regimes of energy and angular momentum. In each case, we have subtracted $\beta J(J+1)$, where β is typically 0.013, in order to be able to display levels of a given vibrational level over a range of J with an expanded energy scale. Calculated $b^3\Pi_2$ levels are not shown in these figures because of their large uncertainties.

At relatively low energies, the structure in general resembles that shown in Fig. 10, which includes $v = 0$ of the $A^1\Sigma^+$ state. The rotation parameters for the A -state levels are smaller than for the b state, and thus the slopes of the energy with $J(J+1)$ is less for the levels that are predominantly A state. However, $b^3\Pi_{0+}$ levels are mixed with A -state levels by the

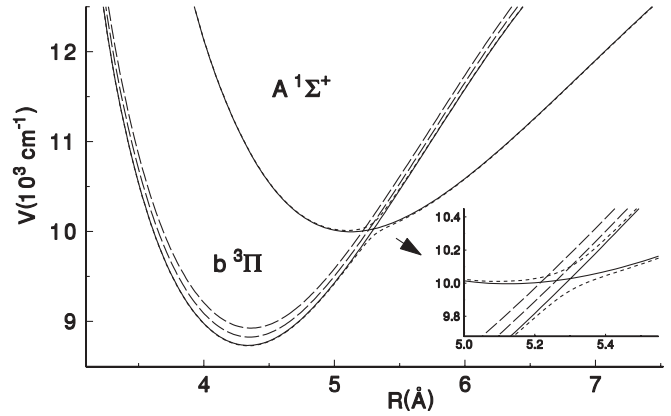


FIG. 8. Potentials for the RbCs $A^1\Sigma^+$ and $b^3\Pi$ states, obtained from fits to the present data set. The diabatic (crossing) potentials for the A state and for $b^3\Pi_0$ are shown as solid lines, the adiabatic potentials as short dashes, while the $b^3\Pi_{1,2}$ potentials, which are the sum of the $b^3\Pi_0$ potential plus spin-orbit functions, are shown with longer dashes.

spin-orbit interaction, and therefore their rotational structure has a smaller slope than that of the $b^3\Pi_1$ levels. Note that three $b^3\Pi_{0+}$ levels ($v = 25-27$) cross the $A^1\Sigma^+ v = 0$ level. These are the lowest $b^3\Pi_{0+}$ levels observed in this study.

The behavior shown in Fig. 10 differs from that displayed at higher energies, such as shown in Fig. 11. While the levels with steepest slope vs. $J(J+1)$, the $b^3\Pi_1$ levels, are unaffected, in the higher-energy regime, the 0^+ levels from $A^1\Sigma^+$ and from $b^3\Pi_{0+}$ are much more highly mixed, so they have approximately the same slope and do not exhibit the narrow avoided crossings as they do in Fig. 10. Figures 12(a) and 13(a) show the quality of the fit over selected regions included in the previous two figures. Data for the higher-energy regime is available primarily from Brazil/LAC and exhibits larger fit residuals than the data from Riga. Figure 13 applies to the two levels that at $J = 0$ tend to energies of 11066 and 11075 cm^{-1} .

Figures 12(b) and 13(b) show the fractional composition of the observed term values, for the selected levels in the

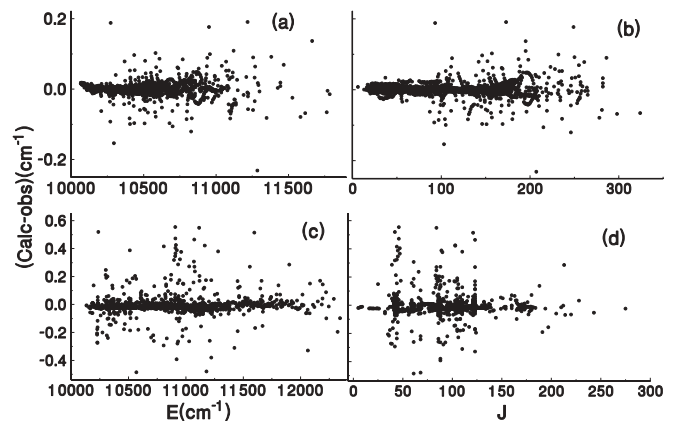


FIG. 9. Residuals from the fit for the two data sets, as a function of energy and J , to show trends in each case. (a) and (b) represent the fits to the data from Riga; (c) and (d) give residuals for the data from Brazil.

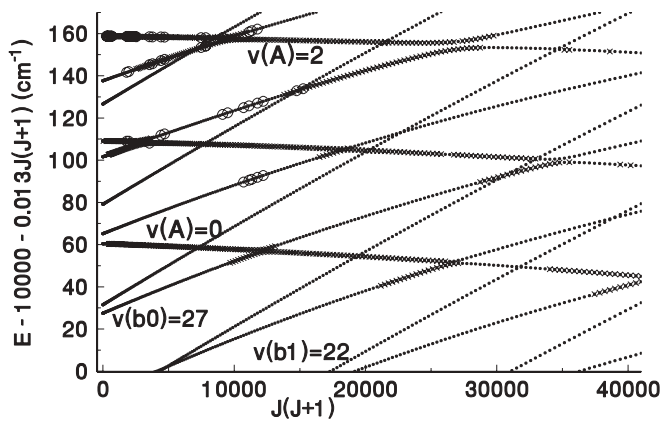


FIG. 10. “Reduced” term values [with $0.013J(J+1)$ subtracted] in the region $v_A = 0$ to 2, for $^{85}\text{Rb}^{133}\text{Cs}$. Small dots are calculated term values; the \times symbols (open circles) denote data from Latvia (Brazil).

low-energy and higher-energy regimes, respectively. For levels nominally $v_A = 2$, the singlet fraction is typically about 80%, except at avoided crossings. In Figs. 11 and 13, the mixing between A and $b^3\Pi_{0+}$ levels is so extensive that vibrational numbering cannot be meaningfully established. For example, at low J , these two nearby levels both have more than 50% A character.

An important issue in this study is the fine structure splitting of the $b^3\Pi$ state. The narrow avoided crossings in the rotational progressions between the mixed 0^+ states and the $b^3\Pi_1$ levels provide relevant information. To discuss these avoided crossings we show first a somewhat finer energy scale for the data near $v_A = 2$ in Fig. 14. The larger avoided crossings are between 0^+ levels. Narrow avoided crossings for $v_A = 2$ and other levels are shown in more detail in Fig. 15. From seven such crossing regions, including one for $^{87}\text{Rb}^{133}\text{Cs}$, we have fit parameters for the diagonal spin-orbit function characterizing the splitting between $b^3\Pi_{0+}$ and $b^3\Pi_1$ (see Fig. 16). As discussed below, this fine structure interval is significantly less than that calculated by one of the *ab initio* methods

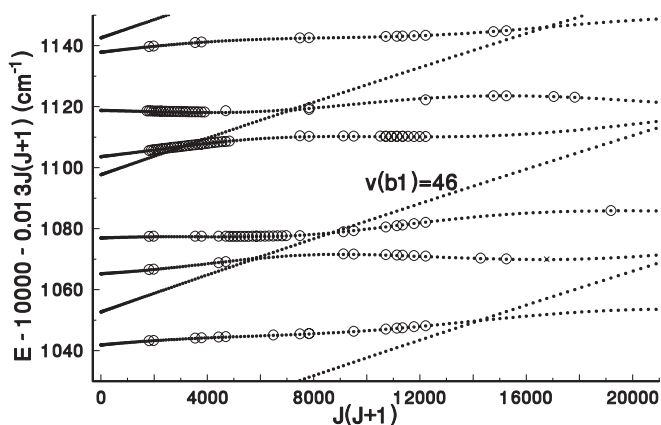


FIG. 11. Reduced term values at higher energy, showing stronger mixing between $A^1\Sigma^+$ and $b^3\Pi_{0+}$ levels. Because of this mixing, vibrational quantum number assignments in this region is not feasible except for the $b^3\Pi_1$ state. Symbols have the same meaning as in the previous figure.

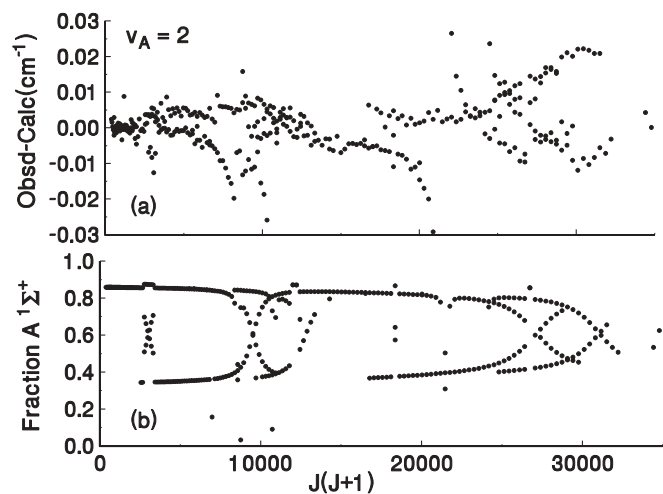


FIG. 12. (a) Residuals in the fit to data for levels near $v_A = 2$. (b) Fraction of $A^1\Sigma^+$ character for levels actually observed in the vicinity of $v_A = 2$.

presented here. Also, several of the term value data points in the avoided crossing regions exhibit residuals between 0.15 and 0.23 cm^{-1} , while in general the rms residual from the data from Riga is 0.02 cm^{-1} , suggesting that the fine structure model could be improved (more extensive data on $b^3\Pi_1$ would of course be useful in this regard). The question arises whether the vibrational numbering of the $b^3\Pi_1$ levels is correctly chosen. If it were one less, than the effective splitting function would be approximately 40 cm^{-1} larger. However, fits that we have made with comparably larger values of $\Delta_{1d}(R)$, scanning over values for the parameters $P_d(1-3)$ in Eq. (4), result in significantly larger residuals over the narrow avoided crossing regions. Repeated efforts to obtain a comparably good fit with a larger amplitude $\Delta_{1d}(R)$ function have not been successful, although there may be some region of parameter space that we have not accessed, that does give a $\Delta_{1d}(R)$ function with a larger minimum amplitude.

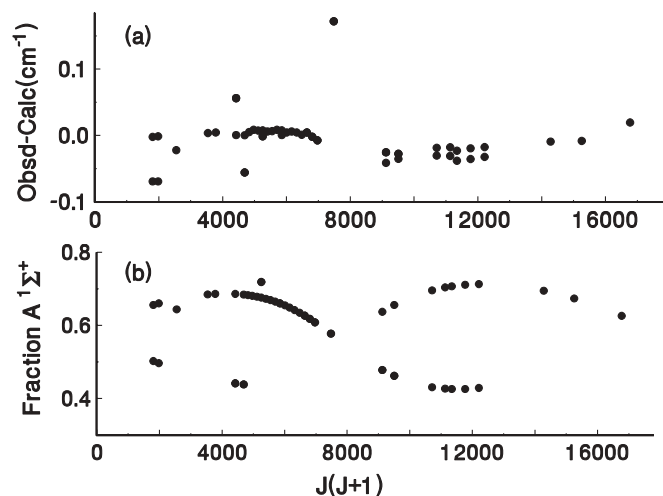


FIG. 13. (a) Residuals in the fit to data for levels with reduced energies between 11060 cm^{-1} and 11085 cm^{-1} . (b) Fraction of $A^1\Sigma^+$ character for levels actually observed in this region.

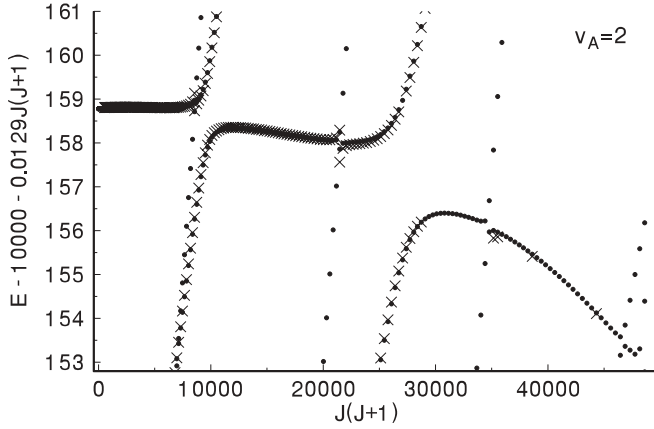


FIG. 14. Zooming in on term values near $v_A = 2$, showing regions of avoided crossing between $\Omega = 0^+$ levels and also between $\Omega = 0^+$ and $b^3\Pi_1$ levels. In this and the following figure, the displayed experimental data, indicated by \times symbols, are entirely from Latvia.

Figure 16 presents the fitted and *ab initio* spin-orbit functions. In each case, the asymptotic value is known from the Cs 6^2P spin-orbit splitting. For the off-diagonal function, $\Delta_{od}(R)$, in Fig. 16(a), the data samples primarily the value of the SO function at the potential crossing point, $R_x = 5.30 \text{ \AA}$, as denoted by a vertical line. This is rigorously true for weak perturbations, according to the principle of stationary phase [55] (PSP), but for a spin-orbit coupling function larger the vibrational energies, one might expect this condition to be relaxed somewhat. In practice, we have varied the $P_{od}(3)$ and fitted $P_{od}(2)$ and $P_{od}(1)$ to fit essentially $\Delta_{od}(R_x)$. With such a procedure, according to PSP, the variance of the fit should be independent of $P_{od}(3)$ so long as $\Delta_{od}(R_x)$ is effectively fixed. In practice, we have found that the $P_{od}(3)$ parameter given in Table III yields the best fit, but values of $P_{od}(3)$ as large as 5.85 \AA (hence closer to the minimum value of the *ab initio*

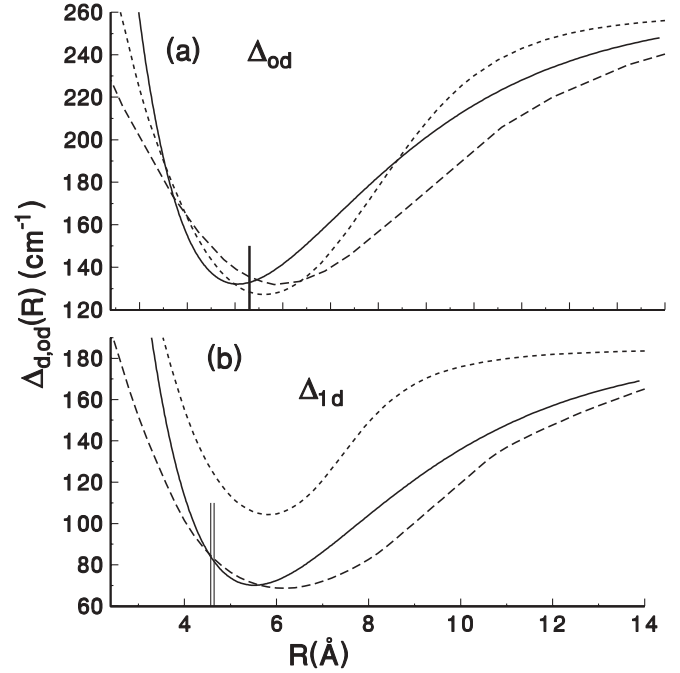


FIG. 16. (a) Off-diagonal and (b) diagonal spin-orbit (bottom) functions. The solid curves denote the fitted functions. The long and short dashed lines are the *ab initio* results obtained by authors (S.K.) (MR-RAS-CI) and (A.V.S.) (ECP-CPP-CI), respectively. The vertical line in (a) denotes the R value of the potential crossing point, while the pair of vertical lines in (b) demarcate the range of $\langle R \rangle$ values for the observed $b^3\Pi_1$ levels.

$\Delta_{od}(R)$ functions) yielded variances only 2% larger than the optimum fitted value.

For the diagonal spin-orbit function, $\Delta_{1d}(R)$, shown in Fig. 16(b), the fit primarily applies to the range of $\langle R \rangle$ values sampled by the observed $b^3\Pi_1$ vibrational functions for the observed avoided crossing regions. We have evaluated these $\langle R \rangle$ values, and found them to lie in a small range around 4.6 \AA , as indicated by the two vertical lines. The range is small because the relevant $b^3\Pi_1$ levels span only a small range in energy.

For comparison with *ab initio* computational results discussed below in Sec. IV, and to estimate the b state $\Omega = 2 - \Omega = 1$ interval, it is relevant to consider the second order spin-orbit (SO2) effects. For this purpose, we take a more general view so as to include all states dissociating to $\text{Rb}(5^2S) + \text{Cs}(6^2P)$. If interactions with states outside those dissociating to $\text{Rb}(5^2S) + \text{Cs}(6^2P)$ can be neglected, the interactions between the A , b , c , and B states (see Fig. 1)

TABLE III. Fitted parameters for the empirical spin-orbit functions, in the form given in Eq. (4). $P_i(1)$ and $P_i(4)$ are in cm^{-1} , $P_i(2)$ are in \AA^{-1} , and $P_i(3)$ are in \AA .

i	Δ_{od}	Δ_{1d}	Δ_{2d}
$P_i(1)$	132.328	71.403	79.000
$P_i(2)$	0.33344	0.31092	0.31464
$P_i(3)$	5.0950	5.50837	5.51913
$P_i(4)$ (fixed)	261.20	184.70	184.70

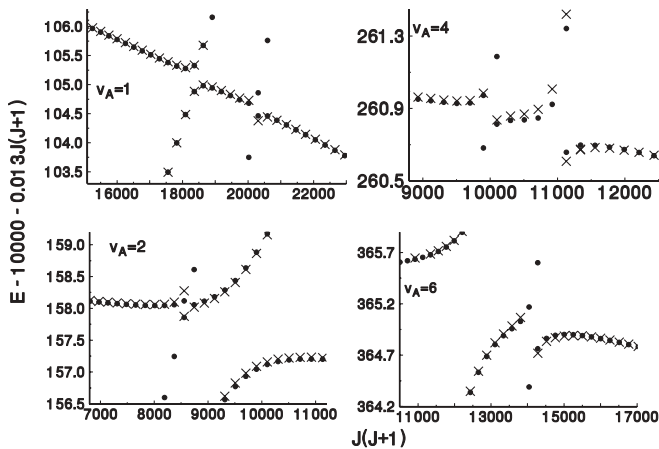


FIG. 15. Detailed view of observed and calculated term values for regions containing avoided crossings between 0^+ levels and $b^3\Pi_1$ levels, over a range of energies and J . In each case, there are also nearby avoided crossings, with larger effective coupling elements, between the two 0^+ levels. The appearance of two term values with the same $J' = 92$ seen for $v' = 2$ corresponds to the appearance of two respective observed spectral lines in Fig. 6

constitute a closed system. We note that there are three $\Omega = 1$ states, namely $b^3\Pi_1$, $c^3\Sigma_1^+$, and $B^1\Pi$. Coupling with the c and B states will lower the effective potential for $b^3\Pi_1$. The two 0^+ states dissociating to $\text{Rb}(5^2\text{S}) + \text{Cs}(6^2\text{P})$, are already included in the Hamiltonian matrix. In the 0^- manifold, there are also two states, namely $b^3\Pi_{0^-}$ and $c^3\Sigma_0^+$. The $\Omega = 1, 0$ interval in the $c^3\Sigma^+$ state reflects primarily SO2 effects because the direct spin-spin interactions are much smaller. In Ref. [17], this interval was experimentally determined to be $9.0(2)\text{ cm}^{-1}$ in $v = 0$. Since there are three coupling functions and one diagonal SO function in the $\Omega = 1$ manifold, and one coupling function each in the two $\Omega = 0^\pm$ manifolds, the situation is experimentally underdetermined. If each of the $\Omega = 1$ functions are equal to each other, and the $\Omega = 0^\pm$ functions are $\sqrt{2}$ times larger, then at $R = 5.255 \text{ \AA}$ (the R_e of the $c^3\Sigma^+$ state), coupling terms of magnitude 84 cm^{-1} will produce the observed 9.0 cm^{-1} $\Omega = 1, 0^-$ interval. As stated above and shown in Fig. 16(b), the mean $\langle R \rangle$ value of the $\Omega = 1$ levels observed in this work is about 4.6 \AA . A SO coupling function of 88 cm^{-1} at 4.6 \AA , which produces a second-order shift of $\approx 3.6\text{ cm}^{-1}$, is compatible with the fitted function of 83 cm^{-1} at $R = 4.6 \text{ \AA}$. In summary, the observed splitting of the $c^3\Sigma^+$ state [17] and the fitted spin-orbit functions observed in this work suggest second-order spin-orbit shifts of $b^3\Pi_1$ of about 4 cm^{-1} . This estimate is used in estimating the $b^3\Pi_2$ - $b^3\Pi_1$ fine structure interval, which is shown in Fig. 8 and included in the four-channel calculations (see Table III below).

IV. AB INITIO COMPUTATION OF THE SPIN-ORBIT COUPLING FUNCTIONS

Coupling of the spin and orbital angular momentum leads to lifting of the $2S + 1$ spin degeneracy of an electronic state of an atom and molecule. This relativistic effect is described by spin-orbit coupling functions or matrix elements. For a molecule these matrix elements at the dissociation limit must be related to the fine-structure splitting of the corresponding atomic states. At short and intermediate interatomic separations, the electrostatic and exchange interactions between the atoms are nonzero and, therefore, the coupling functions between molecular states are R dependent and differ from their asymptotic values.

Here we calculate the diagonal and off-diagonal R -dependent coupling functions of the $A^1\Sigma^+$ and $b^3\Pi$ states of RbCs. Despite the fact that a RbCs molecule is made up of heavy atoms, for most R the energy difference to other $1^1\Sigma^+$ and $3^1\Pi$ electronic states is generally larger than the coupling between the $A^1\Sigma^+$ and $b^3\Pi$ states. Therefore, we can expect that a perturbative treatment in terms of electronic spin-orbit matrix elements is sufficient.

The spin-orbit functions between two electronic wave functions is given by the matrix elements $\langle \Psi' | H_{SO} | \Psi \rangle$, where $|\Psi\rangle$ and $|\Psi'\rangle$ are nonrelativistic wave functions of the $A^1\Sigma^+$ and $b^3\Pi$ electronic states. The operator H_{SO} is the Breit-Pauli Hamiltonian given by

$$H_{SO} = H_{sso} + H_{soo}. \quad (5)$$

The first term on the right-hand side is an one-electron operator that describes the ‘‘spin-same-orbit’’ interaction and in atomic

units is given by

$$H_{sso} = \frac{\alpha^2}{2} \sum_N \sum_i \frac{Z_N}{r_{iN}^3} \vec{l}_{iN} \cdot \vec{s}_i, \quad (6)$$

where the sum N is over all nuclei and the sum i over all electrons, Z_N is the charge of nucleus N , r_{iN} denotes the separation between the i th electron and the N th nucleus, and α is the fine structure constant. The operator \vec{l}_{iN} is the orbital angular momentum between electron i and nucleus N and \vec{s}_i is the spin of electron i . The second term of Eq. (5) describes the ‘‘spin-other-orbit’’ contribution

$$H_{soo} = -\frac{\alpha^2}{2} \sum_{i \neq j} \frac{1}{r_{ij}^3} [\vec{r}_{ij} \times \vec{p}_i] \cdot (\vec{s}_i + 2\vec{s}_j), \quad (7)$$

where the sums i and j are over all electrons, r_{ij} denotes the interelectron separation, and \vec{p}_i is the electron momentum operator.

We have determined the electronic wave function $|\Psi\rangle$ and spin-orbit matrix elements with two different electronic structure methods. The methods are the all-electron multireference restricted-active-space configuration interaction (MR-RAS-CI) [56] and the small-core effective core pseudopotential (ECP) [57] method. The next two subsections describe the essential ingredients of these methods.

A. MR-RAS-CI method

The MR-RAS-CI method partitions the occupied and unoccupied molecular orbitals into subsets: core orbitals, which do not participate in the CI procedure; valence orbitals, which are occupied and allowed to have single, double, and triple excitations; and virtual or unoccupied orbitals, which have at most double occupancy. Since the size of the CI expansion grows quickly with the number of the active space orbitals, we use restrictive measures. The active orbitals are further divided into subgroups with defined number of electrons. We believe that these restrictions do not lead to a significant degradation of the molecular wave function.

The total wave function is a linear combination of many-electron molecular Slater determinants, $|\Phi_\alpha\rangle$

$$|\Psi\rangle = \sum_\alpha C_\alpha |\Phi_\alpha\rangle, \quad (8)$$

The configuration-interaction (CI) coefficients C_α are obtained by solving the generalized eigenvalue problem

$$\hat{H}_{AB} \vec{C} = E \hat{S}_{AB} \vec{C}, \quad (9)$$

where \hat{H}_{AB} is the Hamiltonian matrix for the molecule. The nonorthogonality matrix \hat{S}_{AB} is the overlap matrix of molecular Slater determinants.

At short and long interatomic separations the electrostatic and exchange interactions between atoms in the RbCs molecule changes dramatically, leading to wavefunctions of different character. In order to ensure accurate matrix elements for all R we use different basis sets for short and long range. For $2 \text{ \AA} < R \leq 10 \text{ \AA}$ we use a molecular orbital basis set constructed from Hartree-Fock or Sturm molecular orbitals. Between $10 \text{ \AA} < R < 40 \text{ \AA}$ we use the valence bond configuration interaction method (VB-CI) [56], where the

molecular determinants are constructed from atomic orbitals localized at the atomic centers. These one-electron orbitals are either Hartree-Fock or Sturm functions. Consequently, for large internuclear separations the molecular wave function attains the correct atomic form.

For RbCs, the core, valence, and virtual orbitals are defined as follows. All occupied orbitals up to the $4s^2$ shell in Rb and the $5s^2$ shell in Cs define the core. The core-valence orbitals of the $4p^6$ shell in Rb and the $5p^6$ shell in Cs are included in the active subspace with single and double excitations. The $5s$ and $5p$ valence Hartree-Fock orbitals of Rb and $6s$ and $6p$ orbitals of Cs are added to the active subspace with single, double, and triple occupancy. In addition, we use five s , p , and d virtual Sturm orbitals to complete the active space. Up to double occupancy is allowed for these virtual orbitals. The basis set is constructed from the two reference configurations, Rb $4p^65s$ + Cs $5p^66s$ and Rb $4p^65s$ + Cs $5p^66p$. To restrict the size of the CI matrices we select determinants based on a perturbative estimate of the correlation coefficient of the excited determinants relative to the Rb $4p^65s$ + Cs $5p^66p$ reference configuration. If this coefficient is below a threshold value the corresponding excited configuration is omitted from the CI calculation. The Hartree-Fock or Sturm orbitals for the MO and VB calculation are labeled in the same manner, but it should be realized that they are different spatial wave functions.

Finally, we match the diagonal and off-diagonal spin-orbit coupling matrix elements obtained in the two regions at $R = 10 \text{ \AA}$ and find the curves shown in Figs. 16(a) and 16(b). A discussion of these results is postponed until Sec. V.

B. ECP method

To include relativistic effect in the present study we have replaced the inner core shells of the Rb and Cs atoms by spin-orbit averaged nonempirical small core effective core potentials (ECPs) [57], leaving nine valence electrons (9-ve) of each atom for explicit correlation treatment. In order to monitor the basis set dependence of the present quasirelativistic calculations, both shape- [58,59] and energy- [60,61] consistent ECP basis sets of the alkali metals have been used. The original shape-consistent ECPs of Rb and Cs atoms [62] were augmented by diffuse part of the all-electron basis for electric property calculation [63] and extended by additional diffuse and polarization functions [58,59]. The relevant spin-averaged and spin-orbit Gaussian basis sets used for Rb and Cs atoms were borrowed from the above references.

The molecular orbitals (MOs) of the RbCs derived by self-consistent field (SCF) method were then optimized by the solution of the state-averaged complete active space SCF (SA-CASSCF) problem for the lowest (1-8) $1,3\Sigma^+$ and (1-4) $1,3\Pi$ states taken with equal weights [64]. The dynamical correlation effects were introduced by internally contracted multireference configuration interaction method (MR-CI) [65]. The respective CAS consisted of the 14σ and 10π optimized molecular orbitals. MR-CI was applied for only two valence electrons keeping the rest frozen, i.e., in a full valence (2-ve) CI scheme while the l -independent core-polarization potentials (CPPs) with properly adjusted cutoff radii were

employed to take into account for the rest core-polarization effects implicitly. The ECP SO basis coefficients of both alkali-metal atoms were scaled in order to reproduce experimental fine-structure splitting of the lowest excited Rb(5^2P) and Cs(6^2P) states [66], respectively.

To elucidate impact of electron correlation effect on energies and spin-orbit matrix elements the size-consistent averaged quadratic coupled cluster (MR-AQCC) [67] method was exploited in particular points of internuclear distance as well. In contrast to the above ECP-CPP-CI approach the ECP-AQCC method was applied for explicit correlation of all eighteen core-valence electrons. In this case the respective CAS was restricted by the 8σ and 8π MOs while all single and double excitations from the CAS were included in the MR-AQCC procedure. All calculations were performed by means of the MOLPRO v.2006 program package [68].

V. RESULTS AND CONCLUSION

A. Fitted parameters and term values

As stated above, all experimental term values as well as term values calculated from fitted parameters are presented in the EPAPS files [47], together with numerical functions for the potentials and spin-orbit functions. Table II summarizes the a_i parameters in $V_{BO}(R)$ and the ξ parameter as given in Eq. (2). The number of digits does not signify the absolute accuracy, but are needed to reproduce the potentials and hence the term values to the accuracy of the observations. The parameters that apply for $R < R_L$ and $R > R_R$ are given in Ref. [47]. Table III presents the $P_{d,od}$ spin-orbit parameters. Table IV compares parameters obtained in this work with results of *ab initio* calculations. With regard to the results from Ref. [61] for the $A^1\Sigma^+$ state, we note (in response to a referee's question) that the ion-pair character of this state is very sensitive to the quality of atomic basis set used, and it often requires much more effort in proper accounting of electronic correlation than the valence $b^3\Pi$ state.

B. Franck-Condon factors

In view of the possible application of the information presented here to experiments producing cold molecules from cold atoms via photoassociation and Feshbach resonances, we present in Fig. 17 some of the relevant Franck-Condon factors. Unfortunately, although RbCs Feshbach resonances have been observed by [69], we do not have wave functions for Feshbach resonance states but use instead the wave function for a near-to-threshold ($v = 48$) level of the $a^3\Sigma^+$ state in the top part of Fig. 17. Only the triplet component of the mixed A - b levels contributes to this FC factor, so there large variations from level to level. The lower plots are for transitions between A - b $J = 0$ levels and X state levels of $v = 0$ and 70. It appears that there may be cases in which the same A - b level has moderately favorable FC factors for transitions both to $a(v = 48)$ and $X(v = 0)$, so that a single STIRAP step might suffice to go from a Feshbach resonance to the vibronic ground state, in accord with the proposal in Ref. [2].

TABLE IV. T_e , R_e , and ω_e values for states considered in this study. T_e values are relative to the minimum of the X state. PW—present work

		Ref. and year				PW	
		[42] 2000	[70] 2002	[59] 2005	[61] 2006	ECP	Expt.
T_e (cm ⁻¹)	$b^3\Pi_0$		8630		8976		8732.3(5)
T_e (cm ⁻¹)	$b^3\Pi_1$	8838	8833		8980	8972	8824.9(8)
T_e (cm ⁻¹)	$A^1\Sigma^+$	10065	10160	10132	10870	10174	9996.47(20)
R_e (Å)	$b^3\Pi_0$		4.308		4.294		4.339(1)
R_e (Å)	$b^3\Pi_1$	4.287	4.291		4.293	4.355	4.3513
R_e (Å)	$A^1\Sigma^+$	5.069	4.974	5.16	5.137	5.163	5.1240(3)
ω_e (cm ⁻¹)	$b^3\Pi_0$		52.0		48.43		50.883(1)
ω_e (cm ⁻¹)	$b^3\Pi_1$	53.05	52.8		48.38	50.7	51.06(40)
ω_e (cm ⁻¹)	$A^1\Sigma^+$	37.73	45.9	37.2	36.11	36.5	34.980(3)

C. Open questions and possibilities for future work

The fitted spin-orbit functions can be compared to results from the two independent *ab initio* calculations which are based on very different computational approaches accounting for relativistic effect and electron correlation. Both *ab initio* MR-RAS-CI and ECP-CPP-CI off-diagonal coupling functions Δ_{od} agree very well with their empirical counterpart [see Fig. 16(a)]. Furthermore, when the coupling function from the ECP-CPP-CI method was introduced into the fitting program and other parameters were adjusted by least squares,

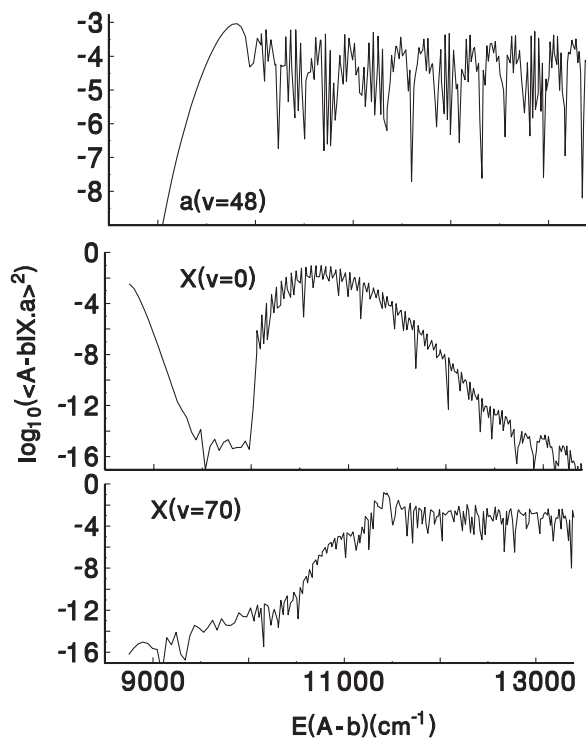


FIG. 17. \log_{10} of Franck-Condon factors for transitions to mixed A - b levels for $J = 0$ of $^{87}\text{Rb}^{133}\text{Cs}$. The top plot applies to a very shallow bound state in the $a^3\Sigma^+$ potential, intended to represent a Feshbach resonance. The middle plot is for $v = 0$ of the $X^1\Sigma^+$ state, and the bottom plot is for $v = 70$ of the X state, which lies 2858.95 cm^{-1} above the minimum of the X state, as compared with the dissociation limit of 3836.13 cm^{-1} .

the variance (the sum of the squares of the residuals divided by the estimated experimental uncertainties) was very nearly the same (within 0.5%) as when the empirical fitted Morse function was used.

However, the present ECP-CPP-CI result for the diagonal spin-orbit function, Δ_{1d} , is systematically higher by 20 to 35 cm^{-1} than both the *ab initio* MR-RAS-CI and the empirical Morse functions [Fig. 16(b)]. We have not able to find a good reason for the pronounced difference in the Δ_{1d} functions. Both Δ_{od} and Δ_{1d} matrix elements obtained in the framework of ECP-CPP-CI method by using of both shape [57,58] and energy [59,61] consistent ECP basis sets coincide with each other within few cm^{-1} . The resulting spin-orbit functions of the ECP-AQCC procedure overestimate their ECP-CPP-CI counterparts by only about of 10–15 cm^{-1} near a minimum of the respective functions. Moreover, the recent implementation of exactly the same ECP-CPP-CI procedure to the A - b complex of NaCs [24], Rb_2 [41], and KCs [71] molecules led to agreement with respective empirical fitted functions within few cm^{-1} . On the other hand, as noted above, the fitting procedure used in this work produced a significantly higher variance when the *ab initio* ECP-CPP-CI Δ_{1d} function was used. It may also be pertinent to note that the empirical values of $\Delta_{1d}(R)$ at the R_e values of $b^3\Pi_1$ in NaCs, KCs, and RbCs, are similar, namely 88, 98, and 93 cm^{-1} , while the corresponding value for RbCs from ECP-CPP-CI is appreciably higher, 128 cm^{-1} . In summary, we choose not to treat *ab initio* results as statistical variables in the usual manner, hence we will not quote an average *ab initio* value for Δ_{1d} or an uncertainty from the difference between the two methods reported here. Very likely one result is nearly correct and the other is only approximately correct. The experimental data on $b^3\Pi_1$, which consists of collisional-induced line progressions, as shown in Fig. 6, leading to avoided crossings in plots of term values vs. $J(J+1)$, as shown in Figs. 14 and 15, is not yet definitive but leads to fits that favor the MR-RAS-CI $\Delta_{1d}(R)$ function. Additional experimental data on $b^3\Pi_1$ levels would clearly be useful.

As reported in Refs. [10,11] photoassociation of laser-cooled Rb and Cs atoms was observed at Yale from approximately 12 cm^{-1} down to 80 cm^{-1} below the Rb $5S + \text{Cs } 6P_{1/2}$ limit, which lies at $15\,014.3\text{ cm}^{-1}$ above the minimum of the X state. Observations of $J = 0$ to 4 levels for approximately 25

0^+ and 0^- bands were used to optimized fits to the long-range potentials. Thus between the data from Brazil and the data from Yale, there is a gap in the data between $12\,350\text{ cm}^{-1}$ and $14\,935\text{ cm}^{-1}$. In this study, we did not attempt to interpolate through the gap, but this could be done, especially with additional data.

Now that many $A^1\Sigma^+-b^3\Pi_{0+}$ levels are accurately known, these mixed singlet-triplet levels might be used as intermediate states to excite higher triplet levels and observe emission, hopefully, to $\Omega = 1$ and 2 levels of the b state. We note however, that the final rms residuals obtained from the fit to the data from both Brazil and from Latvia in some cases, mostly associated with nearby $b^3\Pi_1$ levels, are still larger than the uncertainty of the FTS measurements.

ACKNOWLEDGMENTS

T.B. is grateful for the assistance of H. Salami and G. Bergeman in preparing figures representing the data from Brazil. The work at Stony Brook was supported by NSF Grant PHY0652459. S.K. acknowledges support from AFOSR. A.F.N. acknowledges the CNPq for a grant for doctoral study, and C.E.F. thanks the Instituto Nacional de Optica e Fotonica for support. The work at the University of Latvia was supported by the Latvian Science Council Grant 09.1036. The Riga team is grateful to A. Jarmola for providing the laser diodes built in home made external cavity resonators and to V. Zuters for his help in spectra analysis. The authors from Riga are indebted to A. Pashov for providing the program package for identification and analysis of LIF progressions.

-
- [1] See, for example, L. Li and A. M. Lyyra, *Spectrochim. Acta A* **55**, 2147 (1999) on the use of window states to excite higher triplet states of Li_2 and Na_2 .
- [2] W. C. Stwalley, *Eur. Phys. J. D* **31**, 221 (2004).
- [3] F. Lang, K. Winkler, C. Strauss, R. Grimm and J. Hecker Denschlag, *Phys. Rev. Lett.* **101**, 133005 (2008).
- [4] M. J. Mark, J. G. Danzl, E. Haller, M. Gustavsson, N. Bouloufa, O. Dulieu, H. Salami, T. Bergeman, H. Ritsch, R. Hart, and H.-C. Nägerl, *Appl. Phys. B* **95**, 219 (2009).
- [5] See L. D. Carr, D. DeMille, R. V. Krems, and J. Ye, *New J. Phys.* **11**, 055049 (2009) and other articles in this special issue.
- [6] D. DeMille, *Phys. Rev. Lett.* **88**, 067901 (2002).
- [7] J. M. Sage, S. Sainis, T. Bergeman, and D. DeMille, *Phys. Rev. Lett.* **94**, 203001 (2005).
- [8] K.-K. Ni, S. Ospelkaus, M. H. G. de Maranda, A. Pe'er, B. Neyenhuis, J. J. Zirbel, S. Kotochigova, P. S. Julienne, D. S. Jin, and J. Ye, *Science* **322**, 231 (2008).
- [9] J. Deiglmayr, A. Grochola, M. Repp, K. Mörthbauer, C. Glück, J. Lange, O. Dulieu, R. Wester, and M. Weidemüller, *Phys. Rev. Lett.* **101**, 133004 (2008).
- [10] A. J. Kerman, J. M. Sage, S. Sainis, T. Bergeman, and D. DeMille, *Phys. Rev. Lett.* **92**, 033004 (2004).
- [11] A. J. Kerman, J. M. Sage, S. Sainis, T. Bergeman, and D. DeMille, *Phys. Rev. Lett.* **92**, 153001 (2004).
- [12] K. Pilch, A. D. Lange, A. Prantner, G. Kerner, F. Ferlaino, H.-C. Nägerl, and R. Grimm, *Phys. Rev. A* **79**, 042718 (2009).
- [13] H.-C. Nägerl and J. Danzl (private communication, 2009).
- [14] J. G. Danzl, M. J. Mark, E. Haller, M. Gustavsson, R. Hart, J. Aldegunde, J. M. Hutson, and H.-C. Nägerl, e-print [arXiv:0909.4700](https://arxiv.org/abs/0909.4700) [cond-mat.quant-gas], Sept., 2009.
- [15] S. Ghosal, R. J. Doyle, C. P. Koch, and J. M. Hutson, *New J. Phys.* **11**, 055011 (2009).
- [16] R. Ferber, E. A. Pazyuk, A. V. Stoloyarov, A. Zaitsevskii, P. Kowalczyk, H. Chen, H. Wang, and W. C. Stwalley, *J. Chem. Phys.* **112**, 5740 (2000).
- [17] T. Bergeman, A. J. Kerman, J. Sage, S. Sainis, and D. DeMille, *Eur. Phys. J. D* **31**, 179 (2004).
- [18] A. J. Ross, C. Effantin, J. d'Incan, and R. F. Barrow, *Mol. Phys.* **56**, 903 (1985).
- [19] A. J. Ross, C. Effantin, J. d'Incan, and R. F. Barrow, *J. Phys. B* **19**, 1449 (1986).
- [20] A. J. Ross, R. M. Clements, and R. F. Barrow, *J. Mol. Spectrosc.* **127**, 546 (1988).
- [21] H. Sun and J. Huennekens, *J. Chem. Phys.* **97**, 4714 (1992).
- [22] M. Tamanis, R. Ferber, A. Zaitsevskii, E. A. Pazyuk, A. V. Stoloyarov, H. Chen, J. Qi, H. Wang, and W. C. Stwalley, *J. Chem. Phys.* **117**, 7980 (2002).
- [23] O. Docenko, M. Tamanis, R. Ferber, E. A. Pazyuk, A. Zaitsevskii, A. V. Stoloyarov, A. Pashov, H. Knöckel, and E. Tiemann, *Phys. Rev. A* **75**, 042503 (2007).
- [24] J. Zaharova, M. Tamanis, R. Ferber, A. N. Drozdova, E. A. Pazyuk, and A. V. Stoloyarov, *Phys. Rev. A* **79**, 012508 (2009).
- [25] T. Bergeman, C. E. Fellows, R. F. Gutterres, and C. Amiot, *Phys. Rev. A* **67**, 050501(R) (2003).
- [26] X. Xie and R. W. Field, *Chem. Phys.* **99**, 337 (1985).
- [27] X. Xie and R. W. Field, *J. Mol. Spectrosc.* **117**, 228 (1986).
- [28] C. Linton, F. Martin, I. Russier, A. J. Ross, P. Crozet, S. Churassy, and R. Bacis, *J. Mol. Spectrosc.* **175**, 340 (1996).
- [29] K. Urbanski, S. Antonova, A. M. Lyyra, A. Yiannopoulos, and W. C. Stwalley, *J. Chem. Phys.* **104**, 2813 (1996).
- [30] J. B. Atkinson, J. Becker, and W. Demtröder, *Chem. Phys. Lett.* **87**, 92 (1982).
- [31] C. Effantin, O. Babaky, K. Hussein, J. d'Incan, and R. F. Barrow, *J. Phys. B* **18**, 4077 (1985).
- [32] T.-J. Whang, W. C. Stwalley, L. Li, and A. M. Lyyra, *J. Chem. Phys.* **97**, 7211 (1992).
- [33] Katô, M. Otani, and M. Baba, *J. Chem. Phys.* **89**, 653 (1988).
- [34] P. Qi, J. Bai, E. Ahmed, A. M. Lyyra, S. Kotochigova, A. J. Ross, C. Effantin, P. Zalicki, J. Vigué, G. Chawla, R. W. Field, T.-J. Whang, W. C. Stwalley, H. Knöckel, E. Tiemann, J. Shang, L. Li, and T. Bergeman, *J. Chem. Phys.* **127**, 044301 (2007).
- [35] A. J. Ross, P. Crozet, C. Effantin, J. d'Incan, and R. F. Barrow, *J. Phys. B* **20**, 6225 (1987).
- [36] G. Jong, L. Li, T.-J. Whang, A. M. Lyyra, W. C. Stwalley, M. Li, and J. Coxon, *J. Mol. Spectrosc.* **155**, 115 (1992).
- [37] J. T. Kim, H. Wang, C. C. Tsai, J. T. Bahns, W. C. Stwalley, G. Jong, and A. M. Lyyra, *J. Chem. Phys.* **102**, 6646 (1995).
- [38] M. R. Manaa, A. J. Ross, F. Martin, P. Crozet, A. M. Lyyra, L. Li, C. Amiot, and T. Bergeman, *J. Chem. Phys.* **117**, 11208 (2002).

- [39] C. Lisdat, O. Dulieu, H. Knöckel, and E. Tiemann, *Eur. Phys. J. D* **17**, 319 (2001).
- [40] C. Amiot, O. Dulieu, and J. Vergès, *Phys. Rev. Lett.* **83**, 2316 (1999).
- [41] H. Salami, T. Bergeman, B. Beser, J. Bai, E. H. Ahmed, S. Kotochigova, A. M. Lyyra, J. Huennekens, C. Lisdat, A. V. Stolyarov, O. Dulieu, P. Crozet, and A. J. Ross, *Phys. Rev. A* **80**, 022515 (2009).
- [42] A. R. Allouche, M. Korek, K. Fakherddin, A. Chaalan, M. Dagher, F. Taher, and M. Aubert-Frécon, *J. Phys. B.* **33**, 2307 (2000).
- [43] C. E. Fellows, R. F. Gutterres, A. P. C. Campos, J. Vergès, and C. Amiot, *J. Mol. Spectrosc.* **197**, 19 (1999).
- [44] A. F. Nogueira, C. E. Fellows, and T. Bergeman, *J. Chem. Phys.* **129**, 136101 (2008).
- [45] O. Docenko, M. Tamanis, R. Ferber, A. Pashov, H. Knöckel, and E. Tiemann, *Eur. Phys. J. D* **31**, 205 (2004).
- [46] R. Ferber, I. Klincare, O. Nikolayeva, M. Tamanis, H. Knöckel, E. Tiemann, and A. Pashov, *J. Chem. Phys.* **128**, 244316 (2008).
- [47] See supplementary material at <http://link.aps.org/supplemental/10.1103/PhysRevA.81.042511> for data files associated with this paper.
- [48] R. W. Field and H. Lefebvre-Brion, *The Spectra and Dynamics of Diatomic Molecules*, Elsevier, Amsterdam, 2004.
- [49] D. Colbert and W. H. Miller, *J. Chem. Phys.* **96**, 1982 (1992).
- [50] E. Tiesinga, C. J. Williams, and P. S. Julienne, *Phys. Rev. A* **57**, 4257 (1998).
- [51] C. Samuelis, E. Tiesinga, T. Laue, M. Elbs, H. Knöckel, and E. Tiemann, *Phys. Rev. A* **63**, 012710 (2000).
- [52] R. J. Le Roy, *Can. J. Phys.* **52**, 246 (1974).
- [53] M. Marinescu and H. R. Sadeghpour, *Phys. Rev. A* **59**, 390 (1999).
- [54] D. A. Steck, "Cesium D Line Data", <http://george.ph.utexas.edu/~dsteck/alkalidata>.
- [55] J. Tellinghuisen, *J. Mol. Spectrosc.* **103**, 455 (1984).
- [56] S. Kotochigova and E. Tiesinga, *J. Chem. Phys.* **123**, 174304 (2005).
- [57] M. Dolg, in *Modern Methods and Algorithms of Quantum Chemistry*, edited by J. Grotendorst, John von Neumann Institute for Computing, Jülich, NIC Series, Vol. 1, pp. 479–508 (2000); <http://www.fz-juelich.de/nic-series/>
- [58] S. O. Adamson, A. Zaitsevskii, E. A. Pazyuk, A. V. Stolyarov, M. Tamanis, R. Ferber, and R. Cimiraqlia, *J. Chem. Phys.* **113**, 8589 (2000).
- [59] A. Zaitsevskii, E. A. Pazyuk, A. V. Stolyarov, O. Docenko, I. Klincare, O. Nikolayeva, M. Auzinsh, M. Tamanis, and R. Ferber, *Phys. Rev. A* **71**, 012510 (2005).
- [60] I. S. Lim, P. Schwerdtfeger, B. Metz, and H. Stoll, *J. Chem. Phys.* **122**, 104103 (2005).
- [61] I. S. Lim, W. C. Lee, Y. S. Lee, and G.-H. Jeung, *J. Chem. Phys.* **124**, 234307 (2006).
- [62] R. B. Ross, J. M. Powers, T. Atashroo, W. C. Ermler, L. A. LaJohn, and P. A. Christiansen, *J. Chem. Phys.* **93**, 6654 (1990).
- [63] A. J. Sadlej and M. Urban, *J. Mol. Struct., Theochem* **234**, 147 (1991).
- [64] H.-J. Werner and P. J. Knowles, *J. Chem. Phys.* **82**, 5053 (1985).
- [65] P. J. Knowles and H.-J. Werner, *Theor. Chim. Acta* **84**, 95 (1992).
- [66] NIST Atomic data base; <http://physics.nist.gov/>
- [67] P. G. Szalay and R. J. Bartlett, *J. Chem. Phys.* **103**, 3600 (1995).
- [68] H.-J. Werner, P. J. Knowles, R. Lindh, F. R. Manby, M. Schutz, P. Celani, T. Korona, G. Rauhut, R. D. Amos, A. Bernhardsson, A. Berning, D. L. Cooper, M. J. O. Deegan, A. J. Dobbyn, F. Eckert, C. Hampel, G. Hetzer, A. W. Lloyd, S. J. McNicholas, W. Meyer, M. E. Mura, A. Nicklass, P. Palmieri, U. Schumann, H. Stoll, A. J. Stone, R. Tarroni, T. Thosteinsson, MOLPRO, Version 2006.1, a package of *ab initio* programs.
- [69] K. Pilch, A. D. Lange, A. Prantner, G. Kerner, F. Ferlaino, H.-C. Nägerl, and R. Grimm, *Phys. Rev. A* **79**, 042718 (2009).
- [70] H. Fahs, A. R. Allouche, M. Korek, and M. Aubert-Frécon, *J. Phys. B.* **35**, 1501 (2002).
- [71] A. Kruzins, I. Klincare, O. Nikolayeva, M. Tamanis, R. Ferber, E. A. Pazyuk, A. V. Stolyarov, "Fourier transform spectroscopy and coupled-channels deperturbation treatment of the $A^1\Sigma^+-b^3\Pi$ complex of KCs molecule," *Phys. Rev. A* (accepted, 2010), e-print [arXiv:0912.0644](https://arxiv.org/abs/0912.0644).